LANGMUIR

pubs.acs.org/Langmuir Article

Closest-Packing Water Monolayer Stably Intercalated in Phyllosilicate Minerals under High Pressure

Meng Chen,* Huijun Zhou, Runliang Zhu, Xiancai Lu, and Hongping He

Cite This: *Langmuir* 2020, 36, 618−627 Read Online

ACCESS | Metrics & More | Article Recommendations | Supporting Information

ABSTRACT: The directional hydrogen-bond (HB) network and nondirectional van der Waals (vdW) interactions make up the specificity of water. Directional HBs could construct an ice-like monolayer in hydrophobic confinement even in the ambient regime. Here, we report a water monolayer dominated by vdW interactions confined in a phyllosilicate interlayer under high pressure. Surprisingly, it was in a thermodynamically stable state coupled with bulk water at the same pressure (P) and temperature (T), as revealed by the thermodynamic integration approach on the basis of molecular dynamics (MD) simulations. Both classical and ab initio MD simulations showed water O atoms were stably trapped and exhibited an ordered hexagonal closest-packing arrangement, but OH bonds of water reoriented frequently and exhibited a specific two-stage reorientation relaxation. Strikingly, hydration in the interlayer under high pressure had no relevance with surface hydrophilicity rationalized by the HB forming ability, which, however, determines wetting in the ambient regime. Intercalated water molecules were trapped by vdW interactions, which shaped the closest-packing arrangement and made hydration energetically available. The high pressure−volume term largely drives hydration, as it compensates the entropy penalty which is restricted by a relatively lower temperature. This vdW water monolayer should be ubiquitous in the high pressure but low-temperature regime.

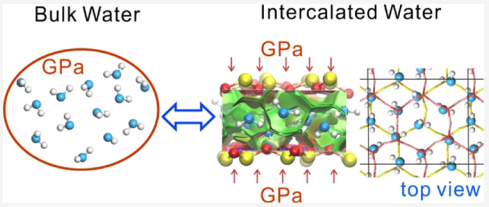

INTRODUCTION

Water is a prerequisite for life, playing a major role in the Earth's geophysical and geochemical cycles, and is crucial for industrial processes.[1] Water is ubiquitous in nature, and yet it possesses many properties that differ qualitatively from most other compounds. The abnormality of liquid water is generally believed to be originated by two different types of structure.[1−5] One is dominated by directional hydrogen bonds (HBs), exhibiting a tetrahedral ice-like structure. The other is mainly constructed by van der Waals (vdW) interactions between molecules with broken HBs. Above the liquid−liquid critical point which lies in the supercooled region,[6] a coexistence of these two types of structure has long been suggested,[4,7] although there have always been doubts about it.[8] Specifically, in the high-pressure regime, vdW interactions are dominant in liquid water. A neutron diffraction study showed oxygen−oxygen pair-correlation function of bulk liquid water at 6.5 GPa and 670 K is strikingly similar to that of liquid Ar, implying it resembles a vdW fluid.[9] A study along the melting curve of liquid water by in situ X-ray diffraction showed that above 4 GPa, the coordination number of water almost remains constant to be approximately 12, while the intermolecular distance shrinks with further compression.[10] Thus, in this regime, water behaves like a simple liquid in which molecules are arranged in a closest-packing structure.

Properties of water in confinement are more complex, depending on confining geometry and surface chemistry.[11−13] The directional HB forming ability of water produces an ice-like monolayer or bilayer in planar hydrophobic confinement from the supercooled to ambient regimes.[14−19] In hydrophilic confinement as generally characterized by an extended HB network connecting the surface and water, low-dimensional ice can be supported or suppressed, depending on surface chemistry, temperature (T), and pressure (P).[20−23] A recent study shows that at room temperature, the ice-like aqueous layer confined between muscovite mica and graphene melts as the pressure is raised above 6 GPa.[22] This pressure-induced phase transition is probably related to the specific water property at high pressure.

Understanding the property of confined water and how it is coupled to external environments bears the potential for the fabrication of novel nanofluidic devices.[24−26] Besides, in Earth science, revealing the partition between water trapped in pores or intercrystalline boundaries[27−29] and that in free fluid is the basic for disclosing the water cycle in the Earth's interior.[30,31] The hydration capacity between two confining surfaces at ambient conditions has been shown to be dependent on the combination of hydrophilicities of the surfaces.[32,33] Hydrophilicity is generally quantified by the contact angle of a water droplet on a surface at ambient conditions.[34,35] From the structural point of view, the hydrophilicity of a silica surface is determined by the hydrogen-bonding ability of the surface, as

Received: October 31, 2019
Revised: December 20, 2019
Published: December 30, 2019

https://dx.doi.org/10.1021/acs.langmuir.9b03394
Langmuir 2020, 36, 618−627

influenced by the density and arrangement of surface hydroxyl (OH) groups.[36,37] However, this hydrophilic and hydrophobic division is in the ambient regime, in which directional HBs of water play an important role. In the high-pressure regime, since vdW interactions are more important, the situation may be different.

A recent experimental study shows that at a subduction-channel condition (2.7 GPa and 473 K), water molecules from the bulk phase are partitioned into kaolinite interlayers.[29] This result recalls the finding of hydrated talc at 6.7 GPa and 923 K.[38,39] Kaolinite and talc are phyllosilicate minerals or, in other words, natural layered materials. The interlayer surface of phyllosilicates is similar to a silica surface in some ways. The interlayer of kaolinite is confined by a hydrophilic aluminum-hydroxide surface and hydrophobic siloxane surface,[40] while that of talc is confined by two hydrophobic siloxane surfaces (Figure 1a,c). No intercalated water has been found in kaolinite and talc under ambient conditions, thus implying that the combination of surface hydrophilicities is unable to support interlayer hydration. The surprising finding of hydrated kaolinite and talc in the high-pressure regime implies a different hydration mechanism.

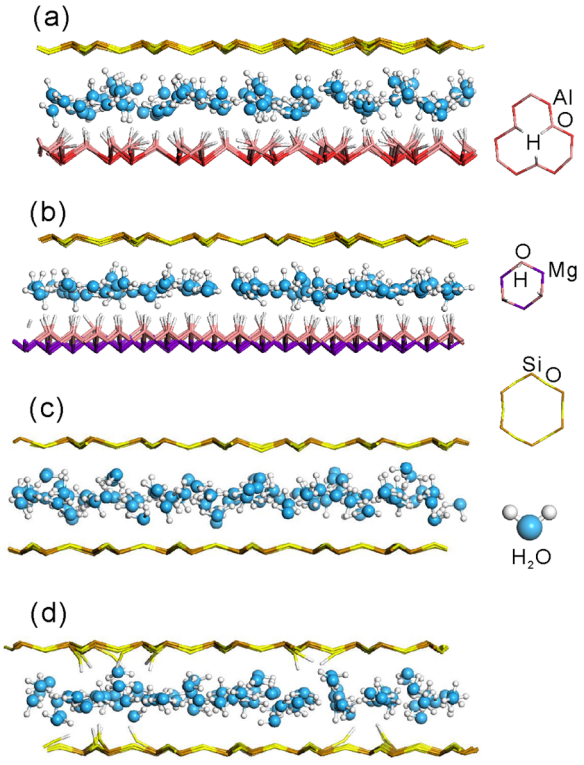

Figure 1. Models of water intercalated in kaolinite (a), lizardite (b), talc (c), and talc with Si vacancies (d).

To answer if the interlayer is stably hydrated, Monte Carlo (MC) simulations in a grand canonical ensemble[41,42] or the thermodynamic integration (TI) approach[43] on the basis of molecular dynamics (MD) simulations is suited. In this study, we derive free energy of water intercalated in phyllosilicates through a TI approach on the basis of MD simulations in the isothermal−isobaric (NPT) ensemble. Kaolinite, talc, and lizardite (a phyllosilicate mineral with interlayers consisting of magnesium hydroxide and siloxane surfaces) are investigated (Figure 1 and Table 1). Because silanol groups accompanying Si vacancies on the surface of talc have been suspected as the reason for hydration,[44,45] talc with and without Si vacancies (Figure 1c,d) are studied at the same time. The pressure and temperature conditions (Table 1) for simulations of kaolinite and talc are consistent with experimental studies,[29,38,44] while that for simulations of lizardite is close to the phase boundary between lizardite and antigorite.[46] This article will show that the decoration of OH groups is irrelevant in determining hydration. Hydration is thermodynamically available at elevated pressure and a relatively lower temperature. The arrangement of stably intercalated water will be shown in the Results and Discussion.

METHODOLOGY

Classical MD Simulations. Descriptions of simulated systems (Figure 1) are summarized in Table 1. The ClayFF force field[47] is used to describe atoms in layers of kaolinite, lizardite, and talc (with and without Si vacancies) with 6 × 3 × 4, 6 × 6 × 4, and 6 × 3 × 4 unit cells, respectively. Water molecules, described by the TIP4P/2005 model,[48] are inserted into the enlarged interlayer space of phyllosilicate minerals. TIP4P/2005 is one of the best water models as it qualitatively reproduces well the phase diagram of water from ambient to high-pressure regimes.[48,49] Although the ClayFF force field is originally developed with the SPC model,[47] the combination of ClayFF and TIP4P delivers similar structural and dynamic properties to that of ClayFF and SPC.[50] Especially, the combination of ClayFF and TIP4P/2005 works better in predicting the diffusion coefficient of intercalated water.[51] The number of water molecules (n) per chemical formula (Table 1) ranges from 0.0 to 3.3. NPT simulation time is more or less 80 ns for each system. At the beginning, each dimension of the supercell is scaled independently to equilibrate the crystal structure. This run proceeds for 25−35 ns. During the latter simulation, only the z-dimension of the supercell is scaled (NP_zT ensemble) and an equilibrated interlayer spacing is achieved. Data are saved every 0.1 ps in the last 10 ns simulation for structural analysis. The time step for simulations is 1 fs. A bulk water phase, as a coupled state, is also simulated under the same temperature and pressure conditions. Simulations are performed with the GROMACS 5.1 package.[52] More details on force fields and MD simulation settings can be seen in Section S1 of the Supporting Information.

Chemical Potential Calculations. Given water partitioned between an intercalated and bulk state (Figure 2a), μ_{int} and μ_w are defined as chemical potentials of intercalated and bulk water, respectively. When water is stably intercalated, $\mu_{int} = \mu_w$, i.e., $\Delta\mu = 0$. The chemical potential μ of either intercalated or bulk water can be separated into two terms

$$\mu = \mu^{I} + \mu^{\times} \quad (1)$$

where the first term is the chemical potential of the isolated (ideal gas) state and the latter the excess chemical potential. μ^I depends on density ρ

$$\mu^{I} = k_B T \ln \rho + C \quad (2)$$

where C is a constant related to the internal partition function of an isolated molecule.[53] The excess chemical potential $\mu^\times$, which is the solvation free energy of a water molecule, is derived with the TI procedure. δN water molecules are arbitrarily selected from the equilibrated configuration. $\lambda = 0$ is coupled to the state with full Lennard-Jones (LJ) and

https://dx.doi.org/10.1021/acs.langmuir.9b03394
Langmuir 2020, 36, 618−627

Table 1. Descriptions of Simulated Systems

	kaolinite	lizardite	talc	talc with Si vacancies
abbreviation	Kln	Lz	Tlc	Tlc_v
chemical formula	$Al_2Si_2O_5(OH)_4{\cdot}nH_2O$	$Mg_3Si_2O_5(OH)_4{\cdot}nH_2O$	$Mg_3Si_4O_{10}(OH)_2{\cdot}nH_2O$	$Mg_3Si_{3.83}O_{9.33}(OH)_{2.67}{\cdot}nH_2O$[a]
simulated conditions	(I) 300 K, 0.1 MPa	(I) 300 K, 0.1 MPa	(I) 300 K, 0.1 MPa	(I) 300 K, 0.1 MPa
	(II) 423 K, 1.3 GPa	(II) 543 K, 1.8 GPa	(II) 923 K, 6.7 GPa	(II) 923 K, 6.7 GPa
	(III) 473 K, 2.7 GPa			
	(IV) 573 K, 3.5 GPa			
stable or metastable n in the formula	(I) 2.78	(I) 2.64	(I) 2.92	(I) 2.78
	(II) 2.78	(II) 2.92	(II) 2.92	(II) 2.92
	(III) 2.92			
	(IV) 2.9			
d_{001} at the stable or metastable hydration state (Å)	(I) 10.64	(I) 10.15	(I) 12.42	(I) 12.51
	(II) 9.67	(II) 9.53	(II) 11.06	(II) 11.07
	(III) 9.43			
	(IV) 9.36			

[a]The chemical formula of talc with Si vacancies corresponds to 1 vacancy in 24 Si sites.[44]

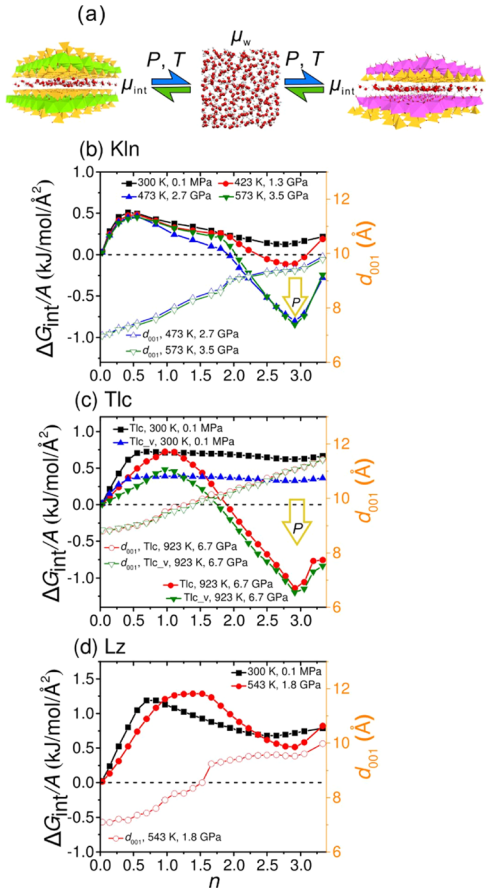

Figure 2. Thermodynamics of hydrated phyllosilicates coupled to a bulk water phase. The schematic of water exchange is shown in panel (a). Intercalation Gibbs free energy ΔG_{int} normalized by lateral area A and d_{001} spacing as functions of water content are shown for hydrated kaolinite (b), talc (c), and lizardite (d). Abbreviations of mineral names can be seen in Table 1.

Coulombic interactions. $\lambda = 1$ is the state in which interactions of selected water molecules are switched off. Intermediate states with $0 < \lambda < 1$ and an interval of $\Delta\lambda = 0.0125$ are introduced, so that there are 81 states in total. States with $0 < \lambda \leq 0.5$ are for switching-off Coulombic interactions, while the rest are for switching-off LJ interactions. The "soft-core" LJ function is used to circumvent the singularity problem.[54] In each state, a stochastic dynamics simulation in NP_zT ensemble is run for 0.3 ns. The last 0.1 ns data are for computing the instantaneous enthalpy derivative $\partial H(\lambda)/\partial\lambda$. $\mu^\times$ is derived through the integration

$$\mu^\times \approx -\frac{1}{\delta N}\int_0^1 \left\langle \frac{\partial H(\lambda)}{\partial \lambda} \right\rangle_\lambda \mathrm{d}\lambda \tag{3}$$

For bulk water, an arbitrary water molecule is selected so that $\delta N = 1$. As for water intercalated in phyllosilicates, an arbitrary molecule is selected from each interlayer. In other words, four water molecules are selected since there are four interlayers. The selected molecule is restrained in the interlayer space in the switching-off simulations. Otherwise, it would cross the solid layer and lead to a free energy bias. The switching-off process is repeated five times and each time a different molecule is randomly selected. $\mu^\times$ and its standard deviation are estimated with the Bennett acceptance ratio (BAR) method.[55]

$\mu^\times_{int}$ and $\mu^\times_w$ are defined as excess chemical potentials of intercalated and bulk water, respectively. Thus, $\Delta\mu$ is expressed as

$$\Delta\mu = \mu^\times_{int} - \mu^\times_w + k_B T \ln \frac{\rho_{int}}{\rho_w} \tag{4}$$

where ρ_{int} and ρ_w are densities of intercalated and bulk water, respectively (see Section S2 and Figure S2 of the Supporting Information for terms in eq 4).

Ab Initio MD Simulations. Ab initio MD simulations are performed with the Born−Oppenheimer scheme by the VASP plane-wave code,[56−58] serving to verify classical simulation results of water arrangements and crystal structures. Models of kaolinite, talc, and lizardite consist of $2 \times 1 \times 1$, $2 \times 1 \times 1$, and $2 \times 2 \times 1$ unit cells in a, b, and c directions, respectively. The intercalated water content n is in accord with that of the stable or metastable hydration state disclosed through the TI procedure, being 3.0 for all of the systems except 2.5 for lizardite at ambient conditions (Table 1). Equilibrium configurations of classical simulations in NPT ensemble are utilized to initiate ab initio simulations. The optPBE-vdW exchange−correlation density functional[59] is used, as it well delivers properties of water and hydrated surfaces,[60,61] and the dispersion correction of the functional is important in describing interactions between nonbonded layers.[62] The

https://dx.doi.org/10.1021/acs.langmuir.9b03394
Langmuir 2020, 36, 618−627

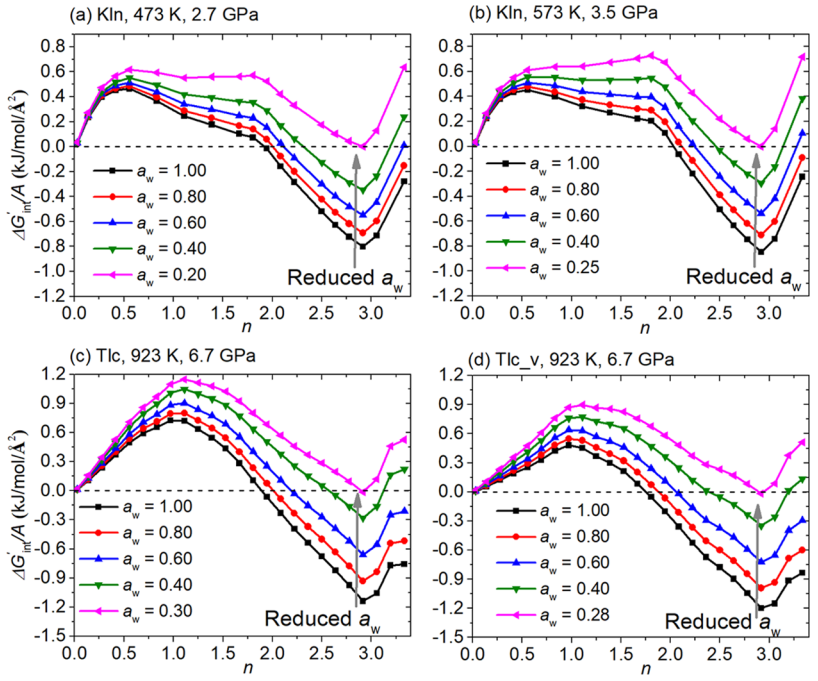

Figure 3. Intercalation Gibbs free energy as a function of water activities.

projector-augmented-wave (PAW) method is used to describe core electrons.[63] Only the gamma point is used to sample the Brillouin zone. Simulations are performed in NPT ensemble for 5 ps at first, to well equilibrate the crystal structure. The energy cutoff of the plane-wave basis set is 800 eV for NPT runs. Then, 10 ps simulations in the canonical (NVT) ensemble are performed with an energy cutoff of 600 eV. Data are collected in the latter 8 ps for analysis. The time step is 0.5 fs. The comparisons of crystal structural parameters between experimental, classical, and ab initio results are shown in Table S2 of the Supporting Information.

RESULTS AND DISCUSSION

Gibbs Free Energy of Hydration. Given water stably partitioned between an intercalated and bulk state, $\Delta\mu = 0$. However, $\Delta\mu = 0$ could also correspond to a transition or metastable state. Thus, the intercalation Gibbs free energy ΔG_{int} is introduced

$$\Delta G_{int} = \int_0^N \Delta\mu(N')\mathrm{d}N' \tag{5}$$

where N is the number of intercalated water molecules. A phyllosilicate mineral without intercalated water ($n = 0$) is the reference state. Thus, a negative ΔG_{int} implies water can be stably trapped into phyllosilicates from the bulk phase (Figure 2). The thermodynamic stabilities of hydrated kaolinite and talc in the high-pressure regime are manifested (Figure 2b,c). Amazingly, the minima for hydrated kaolinite and talc both appear at $n \approx 3.0$ (n is the number of water molecules per chemical formula, Table 1). It is counterintuitive that the introduction of Si vacancies and surface OH groups makes no difference to the stable hydration content of talc, although the energy barrier for hydration is reduced. At ambient conditions, metastable hydrated states for kaolinite and talc are manifested by local free energy minima. Metastable hydrated states are also observed for lizardite (Figure 2d), which bears no stable hydrated state even at high pressure. Metastable states at ambient conditions bear generally lower but close water contents, as compared to stable ones at high pressure (Table 1).

Bulk water with a unity activity is used as the coupled state here. If the coupled state deviates from a bulk phase, e.g., with dissolved components,[64] water activity is reduced. Thus, it could make a difference to hydration. The chemical potential decrement ($\Delta\mu_w$) is related to water activity a_w, as expressed in the following equation[41]

$$a_w = \mathrm{e}^{-\Delta\mu_w/k_BT} \tag{6}$$

The variation in the intercalation Gibbs free energy is related to $\Delta\mu_w$ as shown below

$$\Delta G'_{int}(N) - \Delta G_{int}(N) = \Delta\mu_w \times N \tag{7}$$

where $\Delta G'_{int}$ refers to the intercalation free energy when coupled to water with reduced activity. $\Delta G'_{int}$ as functions of a_w show hydrated states of kaolinite at 473 K and 2.7 GPa and at 573 K and 3.5 GPa are still thermodynamically favorable when water activities are not smaller than 0.20 and 0.25, respectively (Figure 3a,b). The thresholds are 0.30 for talc without Si vacancies and 0.28 with Si vacancies (Figure 3c,d). Thus, at these $P-T$ conditions, hydration is robust for kaolinite and talc in a range of water activities. However, for kaolinite at a lower temperature and pressure (423 K and 1.3 GPa), although $\Delta G_{int}(N)$ of the hydrated state is negative, its absolute value is much smaller (Figure 2b). A water activity less than 0.77 is enough to suppress hydration. It possibly explains why at such a $P-T$ condition kaolinite is not hydrated in experiments,[29] although the kinetic factor could also be responsible. If the absolute value of $\Delta G'_{int}(N)$ is not large enough, a coexistence of hydrated and nonhydrated phases with an equilibrium ratio $K = \exp\left(-\frac{\Delta G'_{int}(N)}{RT}\right)$ is anticipated.

n and d_{001} for hydrated kaolinite at 473 K and 2.7 GPa (n = 2.92, d_{001} = 9.43 Å, Table 1) are in excellent agreement with refining X-ray diffraction data (n = 2.97, d_{001} = 9.44 Å).[29]

https://dx.doi.org/10.1021/acs.langmuir.9b03394
Langmuir 2020, 36, 618−627

However, the d_{001} spacing of the hydrated talc shown here is approximately 11 Å (Figure 2c), which deviates from the previously suggested "10 Å phase".[38,39,44,65] Comodi et al. and Welch et al. reported that n is ∼1.1 in the 10 Å phase.[44,66] At this water content, the d_{001} spacing is close to 10 Å according to our result, but it corresponds to approximately the free energy maximum (Figure 2c), i.e., a transition state. The structural connection between 10 Å and "11 Å phase" verifies that the former is a transition state, as it is characterized by the same layer stacking, and local water packing ways as the latter (Section S6 in the Supporting Information). The transformation from the transitional 10 Å phase into a thermodynamically stable 11 Å phase requires water diffusing into interlayers. As water intercalated in talc hardly diffuses (Section S7 and Figure S11b in the Supporting Information), this transformation is sluggish. Besides, the percentage of water added in experiments ranges from 6 to 15 wt %,[38,39,44] which is just comparable to the water content of hydrated talc disclosed here (12 wt %). Thus, it hardly guarantees the water activity condition. Instead, a coexistence of hydrated 11 Å and nonhydrated phases is anticipated, once the diffusion-controlled transformation is completed. However, due to the limited reaction time, only hydrated talc in the transition state is achieved in experiments. Our study clarifies that the thermodynamically stable state is a 11 Å phase, which bears a similar water content to kaolinite, corresponding to a similar hydration mechanism.

Decomposition of Free Energy Contributions. A thermodynamic route is imagined for the hydration process (Figure 4a): first (step 1), the layer mineral without water experiences a quasi-static isothermal−isobaric expansion process, after which $\Delta G_1 = 0$, because $dG = -S\,dT + V\,dP$ and T and P are constants; second (step 2), the expanded interlayer becomes hydrated, during which ΔU, $-T\Delta S$, and $P\Delta V$ all make contributions to the free energy variation, i.e., $\Delta G_2 = \Delta U - T\Delta S + P\Delta V$. ΔV corresponds to the volume loss of bulk water after intercalation. Thus, the intercalation Gibbs free energy can be decomposed as follows

$$\Delta G_{int} = \Delta U - T\Delta S + P\Delta V \quad (8)$$

Details on deriving terms in eq 8 can be seen in Section S3 of the Supporting Information. Figure 4b shows the respective contributions of ΔU, $-T\Delta S$, and $P\Delta V$ to hydration free energy of kaolinite (contributions to hydrations of other minerals can be seen in Section S3 and Figure S4 of the Supporting Information). ΔU becomes negative as n increases, implying hydration is energetically available. However, it is entropically disfavored. $P\Delta V$ plays a negligible role at ambient conditions, consistent with previous suggestions.[42] As a result, hydration is unavailable at ambient conditions as the entropy effect dominates. However, in the high-pressure regime, $P\Delta V$ plays a significant role, compensating the entropy loss and driving hydration. ΔV accounts for the volume of bulk water with the same number of molecules to intercalated ones, and it just varies slightly from ambient to high-pressure regimes. However, some elevated pressure enhances the $P\Delta V$ term significantly. Thus, this hydration is a pressure-driven event, characteristic above some elevated pressure. Figure 4c shows decompositions of free energy contributions to stable or metastable hydration states with n exhibited in Table 1 under different conditions. Obviously, the stably hydrated talc is also driven by high pressure. In the case of lizardite at 543 K and 1.8 GPa, the $P\Delta V$ term cannot compensate the $-T\Delta S$ term, so that hydration is forbidden. Pressure and temperature play opposite roles, in which the former drives hydration while the latter retards it due to the enlargement of entropy effect. Thus, hydration is in principle available in the high-pressure but low-temperature regime. In addition, it seems counterintuitive that ΔU of the stably hydrated phase is less negative as compared to that of the ambient metastable counterpart. It implies different hydration structures, which will be disclosed in the next section.

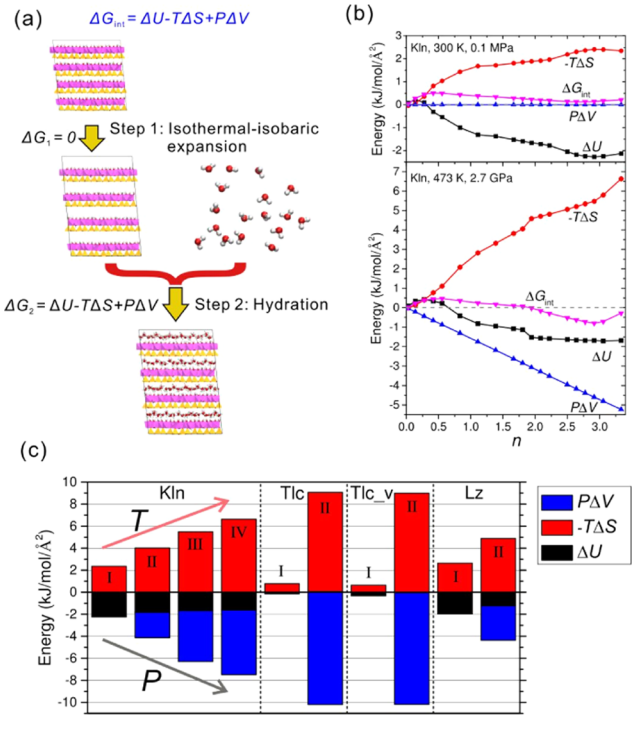

Figure 4. Thermodynamic decomposition results. (a) Route for evaluating contributions to the intercalation Gibbs free energy. (b) Contributions of different terms to free energy of kaolinite hydration. (c) Decompositions of free energy contributions to the stable or metastable hydration states. The Roman numbers correspond to pressure and temperature conditions shown in Table 1.

Arrangement of Water Trapped in the Interlayer. In the ambient regime, a hydrophilic solid surface is generally characterized by an extensive HB network connecting water and surface atoms.[36,37,60,67] Classical simulations show that the metastable state of water trapped in kaolinite in the ambient regime approximately corresponds to the local maxima of tetrahedral order ($Q = 0.66$) and the number of HBs (3.4 HBs per molecule) (Section S4 of the Supporting Information). It indicates a well-developed directional HB network, which is responsible for the large negative ΔU. On the other hand, the stably hydrated phase in the high-pressure regime exhibits less negative ΔU than the ambient metastable counterpart, implying a weaker interaction. This high-pressure stable state bears a disruptive HB network, as manifested by per water molecule forming less than 2.5 HBs and a tetrahedral order lower than 0.35, according to classical simulation results. In cases of talc and lizardite, from ambient to high-pressure regimes, significant decrements of tetrahedral order and number of HBs formed are also observed (Section S4 of the Supporting Information). Ab initio simulations deliver the same trend, although quantitative deviations are observed,

https://dx.doi.org/10.1021/acs.langmuir.9b03394
Langmuir 2020, 36, 618−627

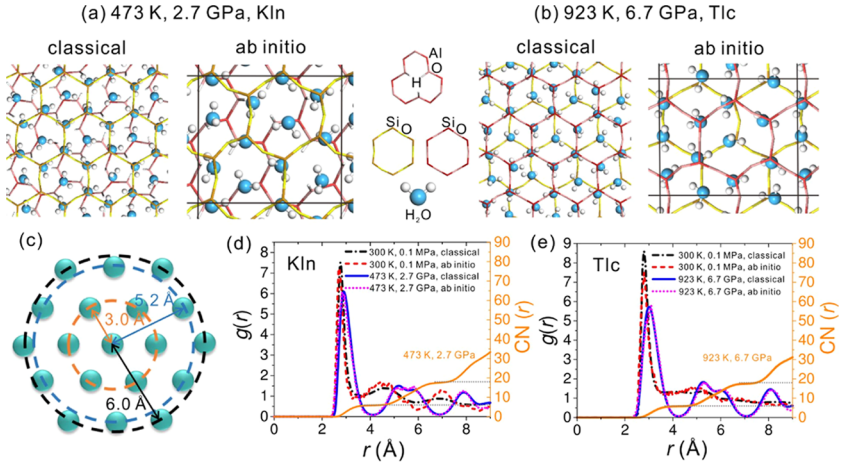

Figure 5. Arrangements of intercalated water disclosed through classical and ab initio simulations. (a) Top views of stably hydrated kaolinite. (b) Top views of stably hydrated talc. (c) A schematic of a closest-packing arrangement. (d) The radial distribution function and coordination number (CN) between O atoms of water intercalated in kaolinite at the stable or metastable hydration state. (e) Same as (d) except for water intercalated in talc.

which is probably due to the hydroxyl group not being restrained in the force field via the bonded term.[68] Thus, the low-dimensional water stably trapped in the interlayer in the high-pressure regime is not supported by directional HBs.

Snapshots of stably trapped water in kaolinite and talc derived through both classical and ab initio simulations manifest a two-dimensional ordered arrangement (Figure 5a,b and Videos S1−S4 in the Supporting Information). This hexagonal closest-packing arrangement is consistent with the X-ray Rietveld refined result.[29] As compared to the hexagonal layer of ice,[69] an extra water molecule enters the center of the hexagon here, making it closest packed. The projection of a water molecule is the vertex or center of a hexagonal silicate ring. Because kaolinite and talc bear similar silicate surfaces, consistent arrangements are observed, which explains the same stable water content ($n \approx 3.0$). Talc with Si vacancies also bears a closest-packing water arrangement (Section S5 and Figure S6b,c of the Supporting Information). The arrangement can be quantified by the radial distribution function $g(r)$ between water O atoms (Figure 5d,e). In the high-pressure regime, the first peak is located at around $r = 3.0$ Å, which is consistent with the distance between adjacent Si atoms. The second and third peaks are around $r = 5.2$ and 6.0 Å, consistent with the prediction of a closest-packing model (Figure 5c). The coordination numbers corresponding to the two minima of $g(r)$ are around 6 and 18, respectively (Figure 5d,e), as also anticipated by the closest-packing model. On the other hand, in the ambient regime, $g(r)$ reflects a disordered packing. The similar water arrangement confined between either surface with or without OH groups in the high-pressure regime shows that hydration is irrelevant to surface hydrophilicity. It is different from the situation in the ambient regime.

Water intercalated in metastably hydrated lizardite at 543 K and 1.8 GPa exhibits a quasi-closest-packing arrangement (Section S5, Figure S6d, and Figure S7c in the Supporting Information). If pressure could be higher, which is not the case for lizardite since the studied condition is already on the phase boundary, a similar perfect hexagonal closest-packing arrangement is anticipated.

To unambiguously identify interactions that shape the water arrangement, the noncovalent interaction (NCI) index[70,71] is calculated on the basis of ab initio electron density ρ. The reduced gradient s is derived with ρ according to $s = \frac{1}{2(3\pi^2)^{1/3}} \frac{|\nabla \rho|}{\rho^{4/3}}$. Noncovalent interactions including HBs and vdW interactions are characteristic of low ρ and s. However, HB interactions correspond to a relatively higher ρ. The sign of the second eigenvalue (λ_2) of the electron-density Hessian matrix $\nabla^2\rho$ distinguishes attractive and repulsive interactions. It is negative for the attractive but positive for the repulsive interactions. In brief, a real-space low-s isosurface with larger ρ and a negative sign (λ_2) indicates HB-like strong attractions, one with larger ρ but a positive sign (λ_2) indicates repulsions, and one with small ρ indicates weak vdW interactions. The isosurfaces for stably hydrated kaolinite and talc (Figure 6) clearly show that water molecules are dominantly surrounded by vdW surfaces, although local HB surfaces are observed. A vdW surface clearly separates the closest water molecules. A water molecule is seen to be trapped in a vdW cage with a faint polyhedron shape. Water interacts with hydroxide surfaces with HBs (Figure 6a) but forms weak vdW interactions with

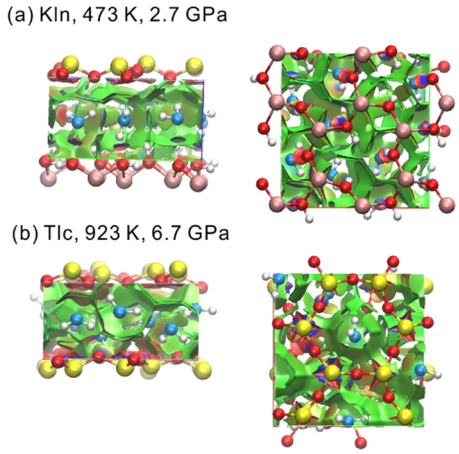

Figure 6. Gradient isosurfaces ($s = 0.6$ au) for hydrated kaolinite (a) and talc (b). The surfaces are colored on a blue-green-red scale according to sign (λ_2)ρ, which ranges from −0.03 to 0.03 au. Blue isosurfaces indicate strong attractions (hydrogen bonds), green ones indicate weak vdW interactions, and red ones indicate a strong nonbonded overlap.

https://dx.doi.org/10.1021/acs.langmuir.9b03394
Langmuir 2020, 36, 618−627

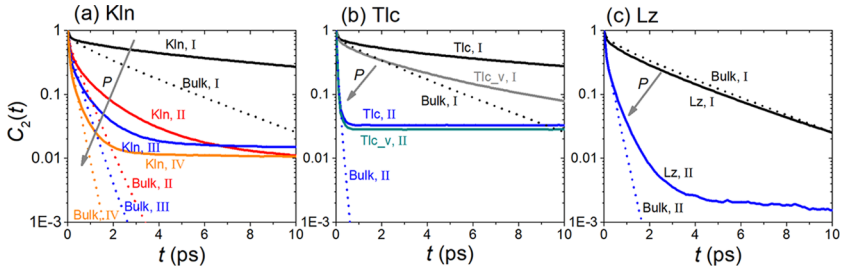

Figure 7. Reorientational time correlation functions of OH bonds of water intercalated in metastably or stably hydrated kaolinite (a), talc (b), and lizardite (c), as compared to those of bulk water at the same conditions. The Roman numbers correspond to pressure and temperature conditions shown in Table 1.

siloxane surfaces. The pore of the silicate ring shapes the vdW surfaces around the water molecule beneath it (Figure 6b). This vdW interaction leads the molecule to locate closer to the pore, giving rise to the puckering arrangement of the water monolayer (see Section S5, Figure S8, and Figure S9 in the Supporting Information). Weak vdW interactions between water molecules, and between water and surfaces, largely shape the water arrangement.

Dynamics of Water Trapped in the Interlayer. In the stable hydration state at high pressure, a water molecule is trapped in a site or, in other words, a vdW cage in the interlayer. A water molecule rarely hops between sites, as disclosed in simulation trajectories (Videos S1−S4 in the Supporting Information). It is reflected in the diffusion coefficient D, which is much lower than that of bulk water at the same conditions (see Section S7 and Figure S11 in the Supporting Information). However, OH bonds of a water molecule are rapidly reorienting, as also shown in simulation trajectories (Videos S1−S4 in the Supporting Information). The reorientation of OH bonds is rationalized by the time correlation function of the OH bond orientation $\boldsymbol{u}$[72]

$$C_2(t) = \langle P_2[\boldsymbol{u}(t_0)\cdot\boldsymbol{u}(t_0 + t)]\rangle \quad (9)$$

where P_2 is the second-order Legendre polynomial, t the time interval, and t_0 the time origin. The average is taken over t_0 based on classical simulation trajectories. In the high-pressure regime, two stages of orientational relaxations of OH bonds of intercalated water are recognized, in contrast to the approximately single exponential decay of $C_2(t)$ at ambient conditions (Figure 7). In the first stage, the relaxation rate is comparable to that of bulk water at the same conditions. However, in the second stage, the relaxation almost stagnates. The first stage represents rapid dangling of OH bonds and switching of HB acceptors. Because a water O atom rarely hops into another site, an OH bond recovers the original orientation after a series of HB switches. The stagnating relaxation in the second stage is rationalized by the orientation reversion. Slowdowns of water reorientations in confinements have been widely reported,[11,73] but the relaxation stagnation shown here is specific for the vdW low-dimensional water. It reflects the decoupling of the rare translational hops and the frequent reorientations. This picture of water dynamics is in accord with the ordered two-dimensional arrangement but disordered orientations of OH bonds. These disordered OH bonds and their rapid reorientations restrict the confinement entropy penalty, in favor of hydration.

Additional Discussions. An ice-like water monolayer or bilayer with an interconnected HB network in hydrophobic confinement has been widely reported.[14−19] One study shows that an ice-like monolayer formation under the ambient confining pressure requires the coupled bulk water being suppressed by external pressure over 1 GPa.[16] Thus, if the confinement and the coupled environment are viewed as one system, it is in a mechanical nonequilibrium state. In contrast, the low-dimensional vdW water shown here is in mechanical and chemical equilibriums with coupled bulk water, as they bear the same chemical potential and are under the same pressure. The formation of a vdW water monolayer is attributed to three aspects: (1) the vdW interactions between water molecules and between water and confining surfaces make the closest-packing arrangement energetically favorable; (2) OH bonds of intercalated water are disordered and reorient frequently, restricting the entropy penalty due to confinement; (3) the elevated pressure−volume term compensates the entropy penalty and drives interlayer hydration. Hydration is in principle favorable in the high pressure but low-temperature regime, which is characteristic of an enhanced pressure−volume term but restricted entropy effect. This pressure-driven hydration is distinct from wetting at ambient conditions, which is just controlled by surface hydrophilicities.[32,33] And yet, the HB forming ability of a surface is almost irrelevant with hydration in the high-pressure regime. Thus, the appearance of a stable vdW water monolayer would not be limited in cases of kaolinite and talc disclosed here and should be ubiquitous in two-dimensional materials regardless of the surface hydrophilicity, if the pressure and temperature conditions are fulfilled. This vdW water monolayer is similar to the three-dimensional vdW water[9,10] also under high pressure.

The pressure-induced melting of the low-dimensional ice-like layer confined between muscovite mica and graphene[22] is probably a transition between ice-like water and vdW water. The relationship between low-dimensional water forms and external factors (surface chemistry, pressure, and temperature) is worth investigating in the future with the methods utilized in this study.

■ CONCLUSIONS

In this study, we disclose a specific form of water monolayer, which is stably trapped in the confining space of phyllosilicate interlayers under high pressure. Unlike the ice-like monolayer in confinement, which is supported by an extended HB network, this monolayer is mainly supported by vdW interactions. It exhibits a closest-packing ordered arrangement but with randomly reorienting water OH bonds. Its formation almost has no relevance with surface hydrophilicities and it is stable in the high-pressure but low-temperature regime. With the approach utilized in this study, revealing the pressure and

https://dx.doi.org/10.1021/acs.langmuir.9b03394
Langmuir 2020, 36, 618−627

temperature boundary above which this water monolayer is stabilized is available and necessary, which would be the future work.

■ ASSOCIATED CONTENT

Supporting Information

The Supporting Information is available free of charge at https://pubs.acs.org/doi/10.1021/acs.langmuir.9b03394.

Descriptions of simulation details; chemical potential differences; terms contributing to the intercalation Gibbs free energy; hydrogen bonding structure and arrangement of intercalated water; structural connection between "10 Å" and "11 Å phase"; diffusion of intercalated water (PDF)

Classical simulation trajectory of water intercalated in stably hydrated kaolinite at 473 K and 2.7 GPa (Video S1) (MPG)

Ab initio simulation trajectory of water intercalated in stably hydrated kaolinite at 473 K and 2.7 GPa (Video S2) (MPG)

Classical simulation trajectory of water intercalated in stably hydrated talc at 923 K and 6.7 GPa (Video S3) (MPG)

Ab initio simulation trajectory of water intercalated in stably hydrated talc at 923 K and 6.7 GPa (Video S4) (MPG)

■ AUTHOR INFORMATION

Corresponding Author

Meng Chen − *Chinese Academy of Sciences (CAS), Guangzhou, China;* orcid.org/0000-0002-1878-2261; Phone: +86-20-85290252; Email: chenmeng@gig.ac.cn

Other Authors

Huijun Zhou − *Chinese Academy of Sciences (CAS), Guangzhou, China, and University of Chinese Academy of Sciences, Beijing, China*

Runliang Zhu − *Chinese Academy of Sciences (CAS), Guangzhou, China*

Xiancai Lu − *Nanjing University, Nanjing, China;* orcid.org/0000-0001-8977-2661

Hongping He − *Chinese Academy of Sciences (CAS), Guangzhou, China, and University of Chinese Academy of Sciences, Beijing, China*

Complete contact information is available at: https://pubs.acs.org/10.1021/acs.langmuir.9b03394

Notes

The authors declare no competing financial interest.

■ ACKNOWLEDGMENTS

This is contribution No. IS-2796 from GIGCAS. This work was financially supported by the National Natural Science Foundation of China (41530313, 41602034, 41921003), Key Research Program of Frontier Sciences, Chinese Academy of Sciences (CAS) (QYZDJ-SSW-DQC023-4), and Youth Innovation Promotion Association CAS. We are grateful to the National Supercomputer Center in Guangzhou for the use of the high-performance computing facility.

■ REFERENCES

(1) Brini, E.; Fennell, C. J.; Fernandez-Serra, M.; Hribar-Lee, B.; Lukšič, M.; Dill, K. A. How Water's Properties Are Encoded in Its Molecular Structure and Energies. *Chem. Rev.* **2017**, *117*, 12385−12414.

(2) Gallo, P.; Amann-Winkel, K.; Angell, C. A.; Anisimov, M. A.; Caupin, F.; Chakravarty, C.; Lascaris, E.; Loerting, T.; Panagiotopoulos, A. Z.; Russo, J.; Sellberg, J. A.; Stanley, H. E.; Tanaka, H.; Vega, C.; Xu, L.; Pettersson, L. G. M. Water: A Tale of Two Liquids. *Chem. Rev.* **2016**, *116*, 7463−7500.

(3) Palmer, J. C.; Poole, P. H.; Sciortino, F.; Debenedetti, P. G. Advances in Computational Studies of the Liquid−Liquid Transition in Water and Water-Like Models. *Chem. Rev.* **2018**, *118*, 9129−9151.

(4) Russo, J.; Tanaka, H. Understanding water's anomalies with locally favoured structures. *Nat. Commun.* **2014**, *5*, No. 3556.

(5) Cuthbertson, M. J.; Poole, P. H. Mixturelike Behavior Near a Liquid-Liquid Phase Transition in Simulations of Supercooled Water. *Phys. Rev. Lett.* **2011**, *106*, No. 115706.

(6) Hestand, N. J.; Skinner, J. L. Perspective: Crossing the Widom line in no man's land: Experiments, simulations, and the location of the liquid-liquid critical point in supercooled water. *J. Chem. Phys.* **2018**, *149*, No. 140901.

(7) Taschin, A.; Bartolini, P.; Eramo, R.; Righini, R.; Torre, R. Evidence of two distinct local structures of water from ambient to supercooled conditions. *Nat. Commun.* **2013**, *4*, No. 2401.

(8) Soper, A. K. Is water one liquid or two? *J. Chem. Phys.* **2019**, *150*, No. 234503.

(9) Strässle, T.; Saitta, A. M.; Godec, Y. L.; Hamel, G.; Klotz, S.; Loveday, J. S.; Nelmes, R. J. Structure of Dense Liquid Water by Neutron Scattering to 6.5 GPa and 670 K. *Phys. Rev. Lett.* **2006**, *96*, No. 067801.

(10) Katayama, Y.; Hattori, T.; Saitoh, H.; Ikeda, T.; Aoki, K.; Fukui, H.; Funakoshi, K. Structure of liquid water under high pressure up to 17 GPa. *Phys. Rev. B* **2010**, *81*, No. 014109.

(11) Thompson, W. H. Perspective: Dynamics of confined liquids. *J. Chem. Phys.* **2018**, *149*, No. 170901.

(12) Cerveny, S.; Mallamace, F.; Swenson, J.; Vogel, M.; Xu, L. Confined Water as Model of Supercooled Water. *Chem. Rev.* **2016**, *116*, 7608−7625.

(13) Zangi, R. Water confined to a slab geometry: a review of recent computer simulation studies. *J. Phys.: Condens. Matter* **2004**, *16*, S5371.

(14) Zangi, R.; Mark, A. E. Monolayer ice. *Phys. Rev. Lett.* **2003**, *91*, No. 025502.

(15) Zangi, R.; Mark, A. E. Bilayer ice and alternate liquid phases of confined water. *J. Chem. Phys.* **2003**, *119*, 1694−1700.

(16) Algara-Siller, G.; Lehtinen, O.; Wang, F. C.; Nair, R. R.; Kaiser, U.; Wu, H. A.; Geim, A. K.; Grigorieva, I. V. Square ice in graphene nanocapillaries. *Nature* **2015**, *519*, 443.

(17) Giovambattista, N.; Rossky, P. J.; Debenedetti, P. G. Phase Transitions Induced by Nanoconfinement in Liquid Water. *Phys. Rev. Lett.* **2009**, *102*, No. 050603.

(18) Han, S.; Choi, M. Y.; Kumar, P.; Stanley, H. E. Phase transitions in confined water nanofilms. *Nat. Phys.* **2010**, *6*, 685.

(19) Bai, J.; Zeng, X. C. Polymorphism and polyamorphism in bilayer water confined to slit nanopore under high pressure. *Proc. Natl. Acad. Sci. U.S.A.* **2012**, *109*, 21240.

(20) Giovambattista, N.; Rossky, P. J.; Debenedetti, P. G. Effect of pressure on the phase behavior and structure of water confined between nanoscale hydrophobic and hydrophilic plates. *Phys. Rev. E* **2006**, *73*, No. 041604.

(21) Yang, J.; Meng, S.; Xu, L. F.; Wang, E. G. Ice Tessellation on a Hydroxylated Silica Surface. *Phys. Rev. Lett.* **2004**, *92*, No. 146102.

(22) Sotthewes, K.; Bampoulis, P.; Zandvliet, H. J. W.; Lohse, D.; Poelsema, B. Pressure-Induced Melting of Confined Ice. *ACS Nano* **2017**, *11*, 12723−12731.

(23) Bampoulis, P.; Siekman, M. H.; Kooij, E. S.; Lohse, D.; Zandvliet, H. J. W.; Poelsema, B. Latent heat induced rotation limited

aggregation in 2D ice nanocrystals. *J. Chem. Phys.* **2015**, *143*, No. 034702.
(24) Severin, N.; Lange, P.; Sokolov, I. M.; Rabe, J. P. Reversible Dewetting of a Molecularly Thin Fluid Water Film in a Soft Graphene−Mica Slit Pore. *Nano Lett.* **2012**, *12*, 774−779.
(25) Yoshida, H.; Kaiser, V.; Rotenberg, B.; Bocquet, L. Dripplons as localized and superfast ripples of water confined between graphene sheets. *Nat. Commun.* **2018**, *9*, No. 1496.
(26) Mouterde, T.; Keerthi, A.; Poggioli, A. R.; Dar, S. A.; Siria, A.; Geim, A. K.; Bocquet, L.; Radha, B. Molecular streaming and its voltage control in ångström-scale channels. *Nature* **2019**, *567*, 87−90.
(27) Sumino, H.; Burgess, R.; Mizukami, T.; Wallis, S. R.; Holland, G.; Ballentine, C. J. Seawater-derived noble gases and halogens preserved in exhumed mantle wedge peridotite. *Earth Planet. Sci. Lett.* **2010**, *294*, 163−172.
(28) Ono, S.; Mibe, K.; Yoshino, T. Aqueous fluid connectivity in pyrope aggregates: Water transport into the deep mantle by a subducted oceanic crust without any hydrous minerals. *Earth Planet. Sci. Lett.* **2002**, *203*, 895−903.
(29) Hwang, H.; Seoung, D.; Lee, Y.; Liu, Z.; Liermann, H.-P.; Cynn, H.; Vogt, T.; Kao, C.-C.; Mao, H.-K. A role for subducted super-hydrated kaolinite in Earth's deep water cycle. *Nat. Geosci.* **2017**, *10*, 947.
(30) Faccenda, M. Water in the slab: A trilogy. *Tectonophysics* **2014**, *614*, 1−30.
(31) Sobolev, A. V.; Asafov, E. V.; Gurenko, A. A.; Arndt, N. T.; Batanova, V. G.; Portnyagin, M. V.; Garbe-Schönberg, D.; Wilson, A. H.; Byerly, G. R. Deep hydrous mantle reservoir provides evidence for crustal recycling before 3.3 billion years ago. *Nature* **2019**, *571*, 555−559.
(32) Kanduč, M.; Netz, R. R. From hydration repulsion to dry adhesion between asymmetric hydrophilic and hydrophobic surfaces. *Proc. Natl. Acad. Sci. U.S.A.* **2015**, *112*, 12338−12343.
(33) Kanduč, M.; Schlaich, A.; Schneck, E.; Netz, R. R. Water-mediated interactions between hydrophilic and hydrophobic surfaces. *Langmuir* **2016**, *32*, 8767−8782.
(34) Li, H.; Zeng, X. C. Wetting and Interfacial Properties of Water Nanodroplets in Contact with Graphene and Monolayer Boron−Nitride Sheets. *ACS Nano* **2012**, *6*, 2401−2409.
(35) Zhu, C.; Li, H.; Huang, Y.; Zeng, X. C.; Meng, S. Microscopic Insight into Surface Wetting: Relations between Interfacial Water Structure and the Underlying Lattice Constant. *Phys. Rev. Lett.* **2013**, *110*, No. 126101.
(36) Cyran, J. D.; Donovan, M. A.; Vollmer, D.; Brigiano, F. S.; Pezzotti, S.; Galimberti, D. R.; Gaigeot, M.-P.; Bonn, M.; Backus, E. H. Molecular hydrophobicity at a macroscopically hydrophilic surface. *Proc. Natl. Acad. Sci. U.S.A.* **2019**, *116*, 1520−1525.
(37) Schrader, A. M.; Monroe, J. I.; Sheil, R.; Dobbs, H. A.; Keller, T. J.; Li, Y.; Jain, S.; Shell, M. S.; Israelachvili, J. N.; Han, S. Surface chemical heterogeneity modulates silica surface hydration. *Proc. Natl. Acad. Sci. U.S.A.* **2018**, *115*, 2890−2895.
(38) Fumagalli, P.; Stixrude, L.; Poli, S.; Snyder, D. The 10Å phase: A high-pressure expandable sheet silicate stable during subduction of hydrated lithosphere. *Earth Planet. Sci. Lett.* **2001**, *186*, 125−141.
(39) Chinnery, N. J.; Pawley, A. R.; Clark, S. M. In situ observation of the formation of 10 Å phase from talc + H_2O at mantle pressures and temperatures. *Science* **1999**, *286*, 940−942.
(40) Šolc, R.; Gerzabek, M. H.; Lischka, H.; Tunega, D. Wettability of kaolinite (001) surfaces — Molecular dynamic study. *Geoderma* **2011**, *169*, 47−54.
(41) Tambach, T. J.; Hensen, E. J.; Smit, B. Molecular simulations of swelling clay minerals. *J. Phys. Chem. B* **2004**, *108*, 7586−7596.
(42) Whitley, H. D.; Smith, D. E. Free energy, energy, and entropy of swelling in Cs−, Na−, and Sr−montmorillonite clays. *J. Chem. Phys.* **2004**, *120*, 5387−5395.
(43) Kanduč, M.; Netz, R. R. Atomistic simulations of wetting properties and water films on hydrophilic surfaces. *J. Chem. Phys.* **2017**, *146*, No. 164705.
(44) Welch, M.; Pawley, A.; Ashbrook, S.; Mason, H.; Phillips, B. Si vacancies in the 10-Å phase. *Am. Mineral.* **2006**, *91*, 1707−1710.
(45) Phillips, B. L.; Mason, H. E.; Guggenheim, S. Hydrogen bonded silanols in the 10 Å phase: Evidence from NMR spectroscopy. *Am. Mineral.* **2007**, *92*, 1474−1485.
(46) Guillot, S.; Schwartz, S.; Reynard, B.; Agard, P.; Prigent, C. Tectonic significance of serpentinites. *Tectonophysics* **2015**, *646*, 1−19.
(47) Cygan, R. T.; Liang, J.-J.; Kalinichev, A. G. Molecular models of hydroxide, oxyhydroxide, and clay phases and the development of a general force field. *J. Phys. Chem. B* **2004**, *108*, 1255−1266.
(48) Abascal, J. L.; Vega, C. A general purpose model for the condensed phases of water: TIP4P/2005. *J. Chem. Phys.* **2005**, *123*, No. 234505.
(49) Aragones, J. L.; Conde, M. M.; Noya, E. G.; Vega, C. The phase diagram of water at high pressures as obtained by computer simulations of the TIP4P/2005 model: the appearance of a plastic crystal phase. *Phys. Chem. Chem. Phys.* **2009**, *11*, 543−555.
(50) Teich-McGoldrick, S.; Hart, D. B.; Gordon, M. E.; Meserole, S. P.; Rodriguez, M. A.; Thurmer, K.; Cygan, R. T.; Yuan, C.; Kimmel, G. A.; Kay, B. D. *Methane Hydrate Formation on Clay Mineral Surfaces*; Sandia National Lab.(SNL-NM): Albuquerque, NM (United States); Pacific, 2015.
(51) Marry, V.; Dubois, E.; Malikova, N.; Breu, J.; Haussler, W. Anisotropy of Water Dynamics in Clays: Insights from Molecular Simulations for Experimental QENS Analysis. *J. Phys. Chem. C* **2013**, *117*, 15106−15115.
(52) Abraham, M. J.; Murtola, T.; Schulz, R.; Páll, S.; Smith, J. C.; Hess, B.; Lindahl, E. GROMACS: High performance molecular simulations through multi-level parallelism from laptops to supercomputers. *SoftwareX* **2015**, *1−2*, 19−25.
(53) Ben-Amotz, D. Interfacial solvation thermodynamics. *J. Phys.: Condens. Matter* **2016**, *28*, No. 414013.
(54) Beutler, T. C.; Mark, A. E.; van Schaik, R. C.; Gerber, P. R.; Van Gunsteren, W. F. Avoiding singularities and numerical instabilities in free energy calculations based on molecular simulations. *Chem. Phys. Lett.* **1994**, *222*, 529−539.
(55) Pohorille, A.; Jarzynski, C.; Chipot, C. Good practices in free-energy calculations. *J. Phys. Chem. B* **2010**, *114*, 10235−10253.
(56) Kresse, G.; Furthmüller, J. Efficient iterative schemes for ab initio total-energy calculations using a plane-wave basis set. *Phys. Rev. B* **1996**, *54*, 11169−11186.
(57) Kresse, G. Ab initio molecular dynamics for liquid metals. *J. Non-Cryst. Solids* **1995**, *192−193*, 222−229.
(58) Kresse, G.; Furthmüller, J. Efficiency of ab-initio total energy calculations for metals and semiconductors using a plane-wave basis set. *Comput. Mater. Sci.* **1996**, *6*, 15−50.
(59) Klimeš, J.; Bowler, D. R.; Michaelides, A. Chemical accuracy for the van der Waals density functional. *J. Phys.: Condens. Matter* **2010**, *22*, No. 022201.
(60) Meier, M.; Hulva, J.; Jakub, Z.; Pavelec, J.; Setvin, M.; Bliem, R.; Schmid, M.; Diebold, U.; Franchini, C.; Parkinson, G. S. Water agglomerates on Fe_3O_4 (001). *Proc. Natl. Acad. Sci. U.S.A.* **2018**, *115*, E5642−E5650.
(61) Gillan, M. J.; Alfè, D.; Michaelides, A. Perspective: How good is DFT for water? *J. Chem. Phys.* **2016**, *144*, No. 130901.
(62) Li, M.; Reimers, J. R.; Dobson, J. F.; Gould, T. Faraday cage screening reveals intrinsic aspects of the van der Waals attraction. *Proc. Natl. Acad. Sci. U.S.A.* **2018**, *115*, E10295−E10302.
(63) Blöchl, P. E. Projector augmented-wave method. *Phys. Rev. B* **1994**, *50*, 17953−17979.
(64) Koop, T.; Luo, B.; Tsias, A.; Peter, T. Water activity as the determinant for homogeneous ice nucleation in aqueous solutions. *Nature* **2000**, *406*, 611−614.
(65) Comodi, P.; Cera, F.; Dubrovinsky, L.; Nazzareni, S. The high-pressure behaviour of the 10 Å phase: A spectroscopic and diffractometric study up to 42 GPa. *Earth Planet. Sci. Lett.* **2006**, *246*, 444−457.

https://dx.doi.org/10.1021/acs.langmuir.9b03394
Langmuir 2020, 36, 618−627

(66) Comodi, P.; Fumagalli, P.; Nazzareni, S.; Zanazzi, P. The 10 Å phase: Crystal structure from single-crystal X-ray data. *Am. Mineral.* **2005**, *90*, 1012−1016.
(67) Björneholm, O.; Hansen, M. H.; Hodgson, A.; Liu, L.-M.; Limmer, D. T.; Michaelides, A.; Pedevilla, P.; Rossmeisl, J.; Shen, H.; Tocci, G.; et al. Water at interfaces. *Chem. Rev.* **2016**, *116*, 7698−7726.
(68) Zhang, G.; Al-Saidi, W. A.; Myshakin, E. M.; Jordan, K. D. Dispersion-corrected density functional theory and classical force field calculations of water loading on a pyrophyllite (001) surface. *J. Phys. Chem. C* **2012**, *116*, 17134−17141.
(69) Hudait, A.; Molinero, V. What determines the ice polymorph in clouds? *J. Am. Chem. Soc.* **2016**, *138*, 8958−8967.
(70) Johnson, E. R.; Keinan, S.; Mori-Sánchez, P.; Contreras-García, J.; Cohen, A. J.; Yang, W. Revealing Noncovalent Interactions. *J. Am. Chem. Soc.* **2010**, *132*, 6498−6506.
(71) Contreras-García, J.; Johnson, E. R.; Keinan, S.; Chaudret, R.; Piquemal, J.-P.; Beratan, D. N.; Yang, W. NCIPLOT: A Program for Plotting Noncovalent Interaction Regions. *J. Chem. Theory Comput.* **2011**, *7*, 625−632.
(72) Laage, D.; Hynes, J. T. A molecular jump mechanism of water reorientation. *Science* **2006**, *311*, 832−835.
(73) Chen, M.; Lu, X.; Liu, X.; Hou, Q.; Zhu, Y.; Zhou, H. Slow dynamics of water confined in Newton black films. *Phys. Chem. Chem. Phys.* **2015**, *17*, 19183−19193.

https://dx.doi.org/10.1021/acs.langmuir.9b03394
Langmuir 2020, 36, 618−627